SPACE WEATHER, VOL. 3, S09B04, doi:10.1029/2005SW000153, 2005

Intercalibration of magnetospheric energetic electron data

R. H. W. Friedel

Los Alamos National Laboratory, Los Alamos, New Mexico, USA

S. Bourdarie

Centre d'Etudes et de Recherches de Toulouse, Département Environnement Spatial, Office National d'Etudes et de Recherche Aérospatiales, Toulouse, France

T. E. Cayton

Los Alamos National Laboratory, Los Alamos, New Mexico, USA

Received 31 January 2005; revised 4 April 2005; accepted 10 June 2005; published 27 September 2005.

[1] The highly energetic electron environment in the inner magnetosphere (geosynchronous orbit and inward) has received a lot of interest recently, as it becomes increasingly evident that existing statistical models such as AE-8 do not capture the range of environmental conditions that exist nor their variability over periods of a solar cycle. Understanding this environment has obvious engineering applications to systems designed to fly in geosynchronous and medium Earth orbits. The detailed understanding of the physics governing the dynamics of highly energetic electrons is a further topic of active research that will eventually lead to global physics-based models capable of now casting or forecasting this environment. For both the development of new statistical models and for the research into the dynamics of highly energetic electrons, the availability of global, well-intercalibrated data is of fundamental importance. We currently have a wealth of inner magnetospheric energetic electron data. This paper presents the current "state of the art" of intercalibrating data from the CRRES, Los Alamos National Laboratory (LANL) GPS, and LANL geosynchronous and Polar energetic electron instruments, covering the period of 1976 to the present (three full solar cycles).

Citation: Friedel, R. H. W., S. Bourdarie, and T. E. Cayton (2005), Intercalibration of magnetospheric energetic electron data, *Space Weather*, *3*, S09B04, doi:10.1029/2005SW000153.

1. Introduction

[2] The natural energetic electron environment in the Earth's radiation belts is of general importance as dynamic variations in this environment can impact space hardware and contribute significantly to background signals in a range of other instruments flown in that region.

[3] There is intense interest in isolating and understanding the mechanisms that contribute to the MeV electron flux buildups in the inner magnetosphere which are frequently observed during the recovery phase of geomagnetic storms. While this is not a new topic, the unprecedented density of observations of relativistic electrons in the inner magnetosphere in the modern era (see Figure 1) has led to new questions and unsolved problems. In a recent review, *Friedel et al.* [2002] covers in detail the current state of research into this topic.

[4] While scientific research into understanding the dynamics of energetic electrons may eventually lead to full physics-based models of the environment, a more basic engineering need is the average or statistical representation of the energetic electron environment suitable for the planning of multiyear missions, particularly as there is a move into more hostile medium Earth orbits such as those occupied by the GPS constellation.

[5] Data from any single point measurement in space has traditionally been used to derive information about the local environment at that satellite. However, both for building statistical models and for researching the dynamics data from multiple spacecraft and multiple instruments needs to be used. Energetic particle detectors have routinely been flown on a range of DOE, NOAA and DOD spacecraft in geosynchronous, GPS and Molniya orbits. Beyond these programmatic missions, this region has also been the subject of purely scientific investigations with current missions such as Cluster (ESA) and Polar (NASA). Data for our work at this point comes primarily from the CRRES MEA [*Vampola et al.*, 1992] Los Alamos National Laboratory (LANL) Geosynchronous SOPA instrument [*Reeves et al.*, 1997] and the LANL GPS energetic particle sensors [*Feldman et al.*, 1985], and from the Polar Comprehensive Energetic Particle and Pitch Angle Distribution (CEPPAD) experiment [*Blake et al.*, 1995]. A time line for

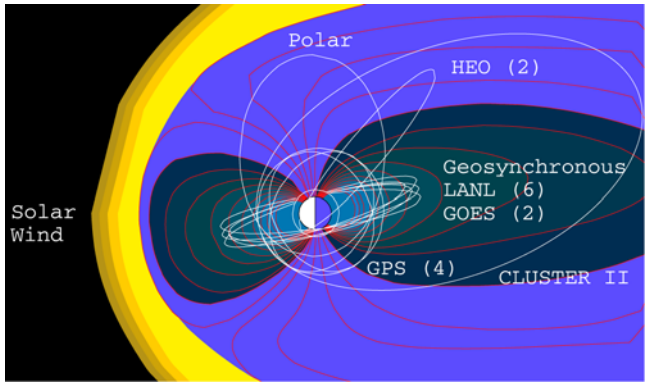

Figure 1. Schematic of current inner magnetosphere missions.

these missions is shown in Figure 2. In what follows we will refer to data from these instruments as simply CRRES, GPS, GEO and Polar.

[6] GEO alone covers 30 years or three full solar cycles, while more global coverage of the inner magnetosphere commences with GPS and CRRES, giving a 20 year coverage or two full solar cycles.

[7] Before the data from these multiple sources can be used for either fundamental research or for building statistical models, they have to be on the "same page"; that is, they have to be properly intercalibrated. In this paper we present the current procedure being used to intercalibrate CRRES, GPS, GEO and Polar. We use the term "intercalibrated" loosely here, since our procedure is not based on physical calibrations of the instruments but on statistics derived from on-orbit data comparisons.

[8] The remainder of this paper is organized as follows: In section 2 we describe in detail the intercalibration procedure used while in section 3 we show a range of examples demonstrating our procedure to our data sets. Section 4 presents a discussion of possible error sources, while in section 5 we show a rigorous scientific test of our intercalibration results as applied to data from geosynchronous orbit. Section 6 reviews some other current usage of the intercalibrated data sets.

2. Data Intercalibration

[9] For all of the applications mentioned in the previous section a basic requirement is the availability of multi-instrument, multispacecraft data that is intercalibrated. Ideally, given "perfect" instrument calibration, no further intercalibration would be required. Energetic electrons represent a challenging measurement task in space, for two reasons: one, it is never possible to fly the amount of shielding required for a "clean" measurement, and two, it

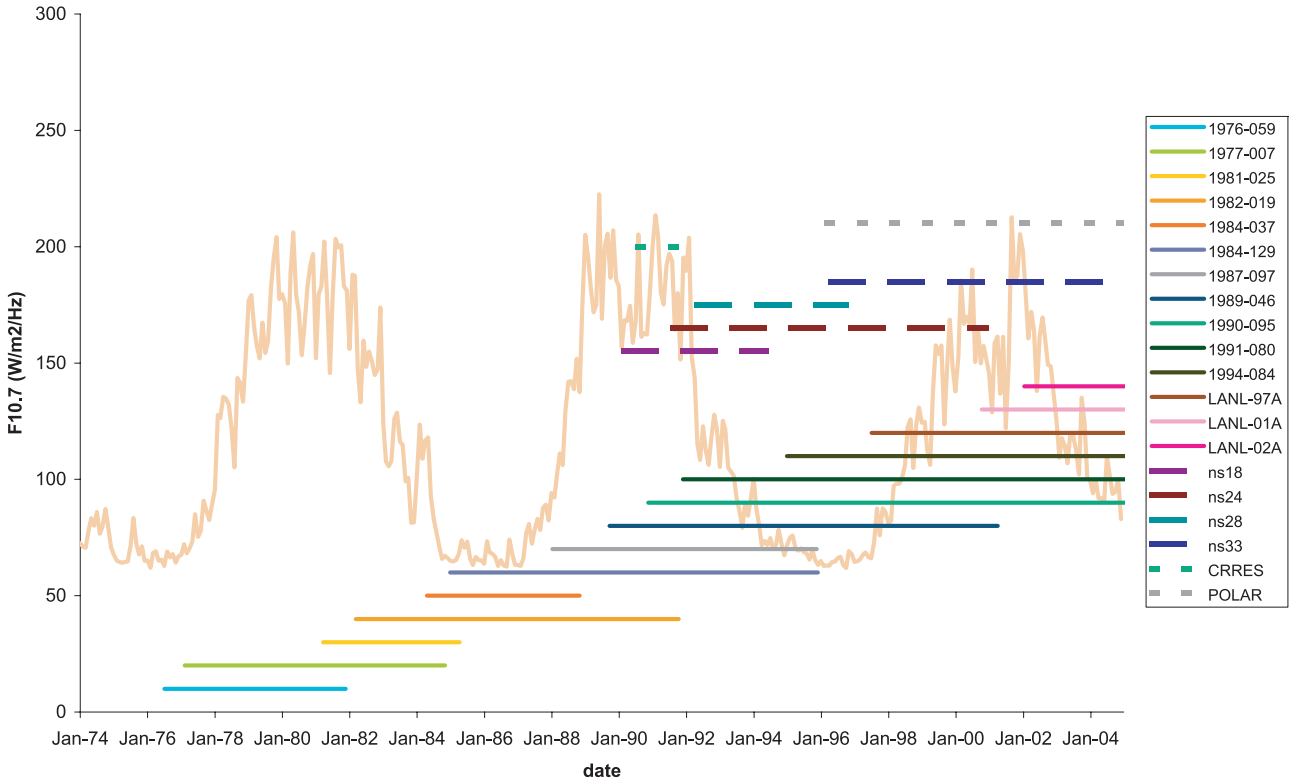

Figure 2. Time line of operation for the 14 GEO (solid lines), 4 GPS (long-dashed lines), and 2 scientific (CRRES and Polar, short-dashed lines) missions used here. The solar cycle phase is indicated by the $F_{10.7}$ solar radio flux curve.

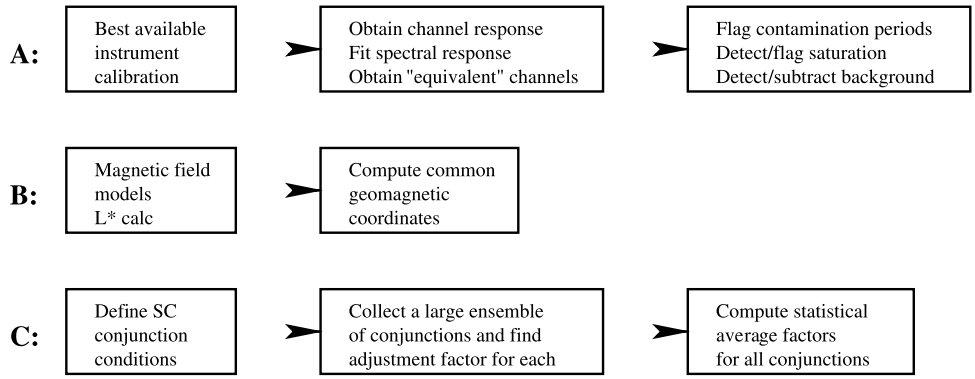

Figure 3. Schematic of intercalibration procedure used.

is impossible to re-create the full energetic particle environment the instrument will encounter in space in the lab for calibrations.

[10] Existing instrument calibrations range from comprehensive to virtually nonexistent. Some have available lab calibrations; those are mainly limited to ''through the aperture'' calibrations which do not address the instruments background response to an omnidirectional, high-energy environment. For some instruments from a series (GPS, GEO) detailed calibrations were only performed for one representative instrument. For other instruments, we only have the ''nominal'' design specifications. Designs of instruments vary widely, with some intrinsically having better immunity to background than others.

[11] While there has been much progress in the modeling of energetic particle instruments from first principle, those methods have their own challenges and still only give factors of 2–5 confidences in an instruments' performance [*Cayton and Tuszewski*, 2005]. Full modeling of these instruments is a time and computer-intensive procedure, and has only been done for a few instruments (GPS, some GEO). These modeling efforts can also tell you for what environments an instrument is likely to perform better or worse, and when it might be in principle impossible to recover a ''clean'' spectrum from an instrument.

[12] Given the limitations of each individual instrument's calibration, we have to resort to further on-orbit calibrations using the actual data collected. As a starting point we use the best available instrument calibrations, some simple assumptions, a great deal of knowledge of the magnetospheric environment and dynamics, and the basic physics of the transport processes for energetic electrons. We have to decide on criteria that tell us when we can compare data between instruments on two spacecraft, and how to propagate these comparisons forward and backward in time. We have to decide on some ''gold standard'' as a basic reference for on-orbit comparisons. Our intercalibration will then consist of a simple scaling of all other instrument's spectra to our common standard.

[13] The basic assumption here is that each instrument measures a representation of a spectrum independent of count rate or spectral hardness, and that our simple scaling addresses uncertainties in each instrument's effective geometric factor and efficiency. We know a priori that some of these assumptions are violated at times [*Cayton and Tuszewski*, 2005], and that they ultimately need to be addressed in each instruments' fundamental response function. However, in the absence of such calibrations we have to start somewhere, and hope to achieve a set of intercalibration factors that are at least valid most of the time. This is an ongoing process, both to incorporate continuing new data sets and to incorporate updated higher-fidelity instrument calibrations as they become available.

[14] Our basic intercalibration procedure is outlined schematically in Figure 3. The procedure is explained for intercalibrating a new instrument on a different spacecraft to the ''gold standard'' instrument. Each step in the process is explained in more details in the sections below.

2.1. Obtaining Sanitized and Comparable Data

[15] Step one is summarized in block diagram A of Figure 3.

2.1.1. Obtaining Channel Response

[16] Starting from the existing calibrated channels of the ''gold standard'' (flux) we fit an exponential spectrum to these channels and evaluate the flux values at the ''target'' instrument channels. This can accommodate both integral and differential ''target'' channels. These will then form the set of equivalent channels for comparison from which a set of adjustment factors will be found.

[17] This fitting process can at times result in nonrepresentative spectra, if there are natural processes acting that cause spectra that deviate substantially from the assumed functional form fitted. Examples of such processes could be substorm-related processes, which can lead to spectral peaks over a limited energy range that cannot be represented by a simple exponential fit. Such time periods are detected by a bad quality of fit and are excluded from the data.

2.1.2. Data Contamination

[18] It is well known that during times of solar energetic proton events (SEPs) many of the detectors used here are

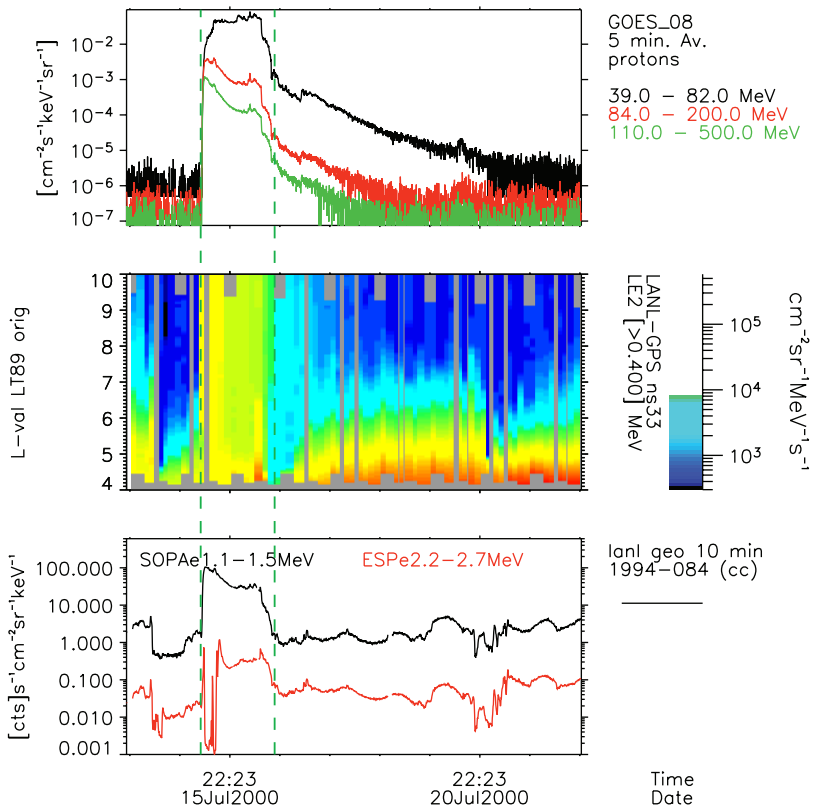

Figure 4. (top) Example of solar energetic particle (SEP) data from GEOS 8 leading to contamination in data from the (middle) GPS and (bottom) GEO instruments. The SEP period is between the two vertical green lines.

contaminated with strong background counts. We use the NOAA GOES energetic proton data to mask out our data during such active times, by monitoring a threshold flux of 10^{-5} ($cm^{-1}s^{-1}sr^{-1}keV^{-1}$) on the 39–82 MeV proton channel. Figure 4 gives an example of a period of solar energetic particle (SEP) contamination. The SEP event is clearly visible in the elevated flux levels of energetic protons measured at GOES 08. These ions can penetrate the electron detectors at GPS and GEO, leading to elevated electron flux observations, across all L values sampled, as clearly shown by the GPS data.

[19] Depending on the instrument there may be regions in the orbit where we know that the data is contaminated by background. This is the case for the Polar CEPPAD imaging electron spectrometer (IES) instrument, where penetrating hard electrons make its data unusable in regions below $L \sim 5.5$.

[20] We simply do not use data from such contaminated periods or regions in our intercalibration procedure.

2.1.3. Background

[21] Background levels due to thermal noise or other contamination such as cosmic rays are present in all particle instruments. These levels can be detected by examining data during intervals when the spacecraft are outside the trapping region for energetic electrons, this occurs over the polar cap on open field lines for GPS and during extreme magnetospheric compression events for the geosynchronous regions. We detect and track these background counts over time and subtract these counts before using the data in our assimilation.

[22] Figure 5 shows the background levels detected for GPS NS18. The GPS orbit routinely leaves the trapping region for energetic electrons because of its inclined orbit, sampling field lines that are no longer closed at large L values. During those times only the background and noise counts are observed. The background can be seen as the low count plateau at the low cumulative probability values (GPS spends approximately 30% of its time in open field line regions).

[23] This observed background level may also depend on time. As silicon detectors or microchannel plates age on orbit and are themselves degraded because of the backgrounds they experience, the background counting rates may increase. The natural cosmic ray background itself has a solar cycle variation. Figure 6 shows the variation of the background levels for GPS NS18 from 1990 to the middle of 1994. As a first step we approximate the background variation in time with a straight line fit.

[24] The background levels are subtracted from the data. In most areas this is a small correction, because the count

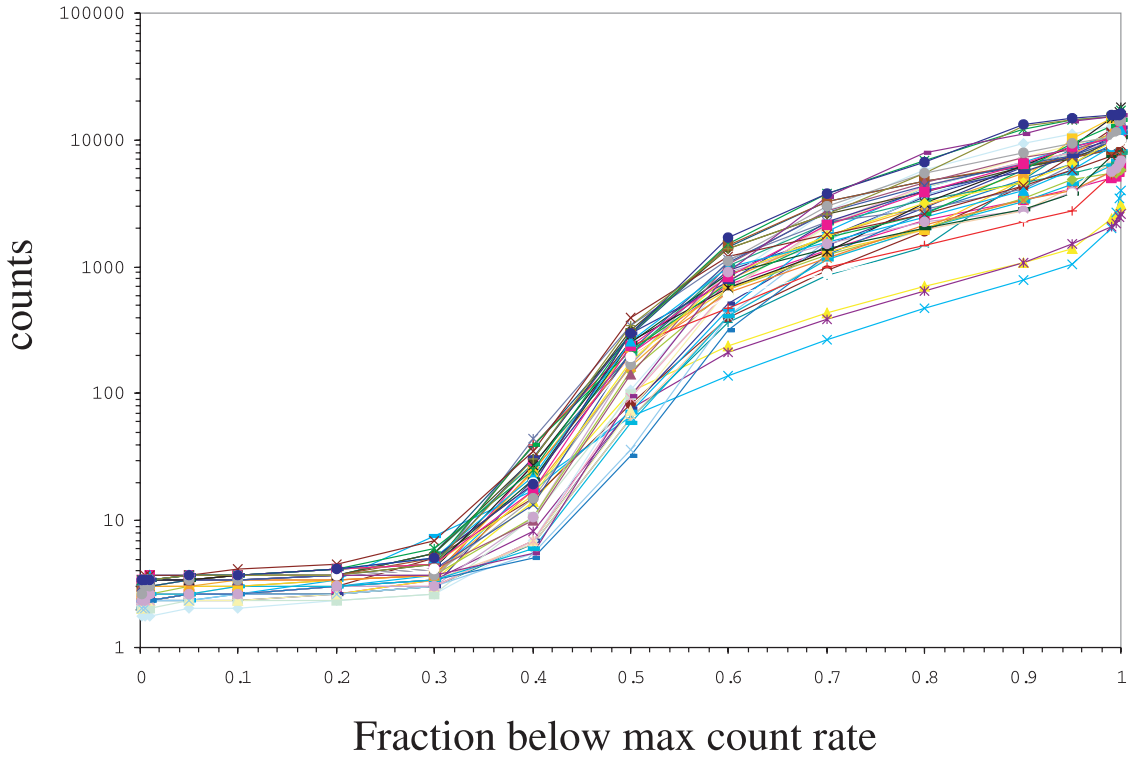

Figure 5. Cumulative probability of observed counts for GPS NS18 for a number of passes through the outer radiation belt. Each colored curve shows for one pass the fraction of observations made at count levels below the maximum count observed during that pass.

rates are generally much higher than the background levels. This correction does become important where the count rates are lower. We use another safety factor and exclude any data that is within a factor of three of the background levels.

2.1.4. Saturation

[25] Data saturation occurs in some instruments as a limit of counting speed during high count intervals, leading to an artificial high plateau in observed counts. These levels are statistically observable and we can ensure that only those data below saturation levels are used in the assimilation process. In Figure 5 saturation effects would manifest as a counting plateau near the high cumulative probability values. Since this is absent, we can conclude that GPS NS18 does not saturate.

[26] Figure 7 shows the fraction of observations of a given flux level (of total observations) for one of the channels on the Polar High Sensitivity Telescope electrons (HISTe) instrument across a range of L values. The high plateau in flux observed in the $L = 4-5$ region, in the center of the radiation belts, is a saturation effect for this instrument. Indicated are also areas of SEP contamination and the background levels of the instrument at high L values, when polar is on open field lines.

[27] Such saturation limits are normally only due to the electronic counting process and are normally stable in time. However, some instruments such as the Polar HIST instrument are thought to have a variable dead time and thus a variable saturation limit. More detailed analysis of the instrument response may recover additional periods of useful data, but that is beyond the scope of the work presented here.

2.2. Geomagnetic Coordinates

[28] Before we can define spacecraft conjunctions we need to establish a common and meaningful coordinate system (summarized in block diagram B of Figure 3). We will make use here of our knowledge of the motion of energetic particles in the inner magnetosphere. In general, any charged particle will undergo gradient and curvature drift because of the inhomogeneous magnetic field, and electric field drift due to the existing electric fields (dawn-dusk, corotation) [*Roederer*, 1974]. For highly energetic electrons the electric field drifts are negligible, and the motion is entirely controlled by the magnetic field. Gradient and curvature drift for electrons combines to produce a circular drift motion counterclockwise around the Earth (viewed looking down on the north pole), leading to so-called "drift shells" that are independent of particle energy and dependent only on the magnetic field topology. The L^* parameter characterizes such drift shells for arbitrary magnetic fields, and represents the equivalent radius of the drift shell at the magnetic equator in a simple dipole field [*Roederer*, 1974] in units of Earth radii. This is an

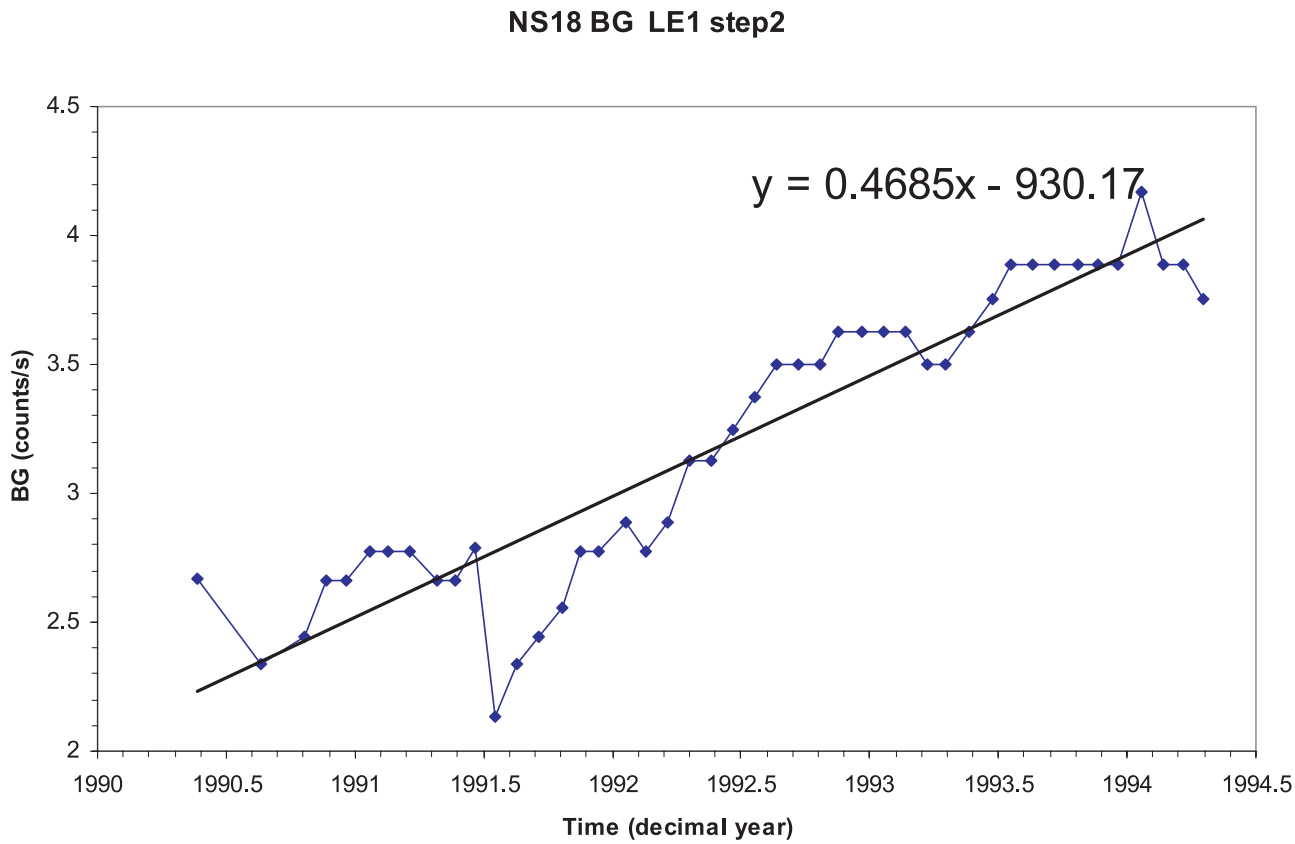

Figure 6. Variation of GPS NS18 background count levels over time.

extremely useful parameter for labeling the position of a measurement, as in the absence of losses and gains particles measured at the same L^* but at different locations in the magnetosphere can be expected to have the SAME flux. This is strictly true for particles at one pitch angle only, as L^* depends on pitch angle. In our present work we use spin-averaged data and a representative L^* calculated for 90° pitch angle. This leads to additional errors as discussed in section 4.2.

[29] We thus compute the same geomagnetic coordinates for all satellites, using the same magnetic field model. Our current choice is static Olson Pfitzer 1977 model [*Olson and Pfitzer*, 1977], which has been shown to be a good average model for the inner magnetosphere [*Jordan*, 1994]. This step can be upgraded to include more realistic, dynamic models at a later stage.

2.3. Adjustment Factors From Spacecraft Conjunctions

[30] A strict definition of a spacecraft conjunction would be based solely on the actual location of two spacecraft, defining a minimum distance between them. Such a definition would however yield a very small or even zero number of conjunctions. We use a more relaxed definition based on the geomagnetic coordinates discussed in the previous section, and on our knowledge of particle motion and magnetospheric activity. Our aim is to obtain a statistically meaningful set of conjunctions that enable the derivation of good adjustment factors between the two instruments under investigation (see block diagram C of Figure 3).

[31] The procedure described here applies to GPS-CRRES, GEO-CRRES and GPS-Polar conjunctions, but not to GPS-GPS and GEO-GEO which never have conjunctions of this nature. For GPS-GPS and GEO-GEO we instead use a long-time average comparisons, since we have many missions in statistically the same orbits.

[32] Referring to Figure 8 we use the following conditions defining a "conjunction.": (1) $L < 6$ and $\Delta L < 0.1$ (for L^*), (2) $\Delta B/B_{EQ} < 0.1$ (close to the magnetic equator), (3) magnetic local time (MLT) within 2 hours of 0600 and 1800, (4) magnetospheric activity quiet ($Kp < 2$ for two days before conjunction, and (5) $\Delta t < 3$ hours.

[33] The first constraint is the most strict, requiring the measurements to be made very close to the same drift shell. The limit on $\Delta B/B_{EQ}$ restricts conjunction to the geomagnetic equator, ensuring that both instruments can sample the same full particle distribution (all particles bouncing along a field line go through the geomagnetic equator). The restriction in local time is due to the use of model magnetic fields in obtaining the required model coordinates (L^*), which perform best in these regions as

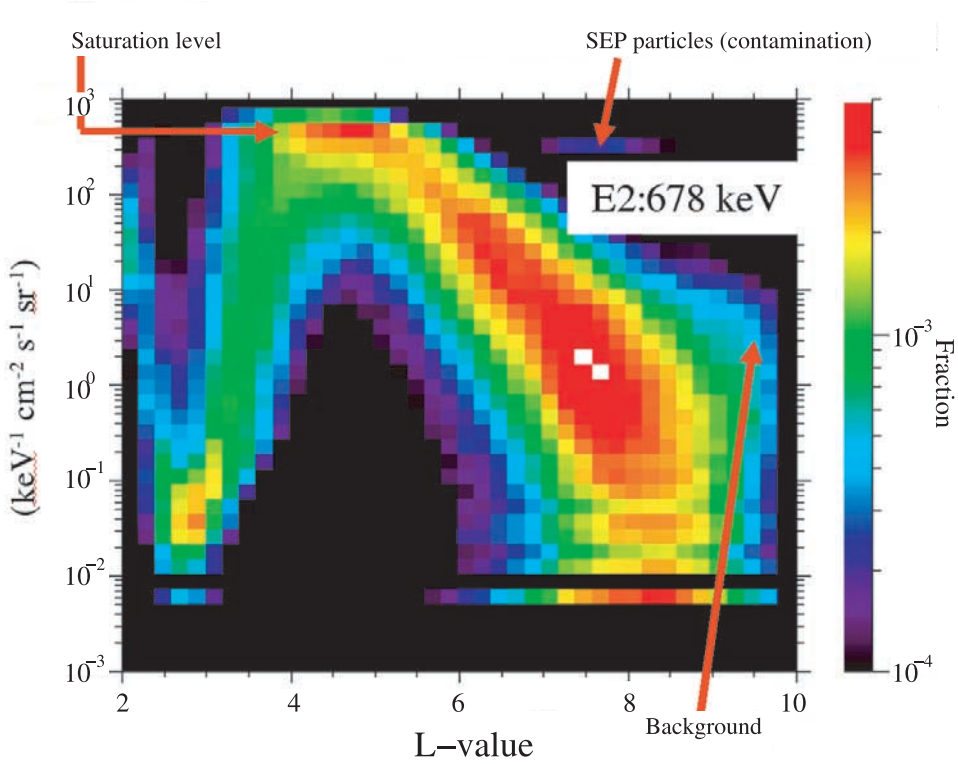

Figure 7. Fraction of observations of a given flux level (of total observations) for the 678 KeV electron channel of Polar HISTe showing the saturation and background levels, plus an example of SEP data contamination.

this excludes compression events around noon and substorm-related dynamics around midnight. The low-activity requirement allows us to relax the time constraint on conjunctions, and allows us to exploit the noon-midnight symmetry of drift shells. During low activity we are less likely to see loss or source events, and electron fluxes are generally uniform in MLT around a drift shell. Furthermore, magnetic field models generally perform better during these times as well, yielding better estimates of L^*.

[34] Once a set of conjunction has been found in this manner we find an adjustment factor for each energy channel that matches the target instrument's data to our gold standard. We collect all these adjustment factors and find a statistical average factor across all conjunctions, ignoring factors outside of one standard deviation.

3. Application of Our Procedure

[35] Figure 9 shows the overall process we used in intercalibrating the data between CRRES, GPS, GEO and Polar. A time line for all the missions used is given in Figure 2.

[36] As mentioned before, our on-orbit calibration procedure relies on having a "gold standard," a reference instrument which is trusted to perform the best and cleanest measurement possible. We chose here the MEA instrument on CRRES, since it was the last scientific instrument to fly in the equatorial region covering the inner magnetosphere from L = 1.2 to 7.5. MEA was a magnetic spectrometer, measuring electrons in the range of 120 KeV to 1.2 MeV. A magnetic spectrometer used magnetic deflection to bend incoming electrons onto a detector, which is an energy selective process. Pulse height analysis for the detectors provided a second energy discriminator, while a background detector that electrons

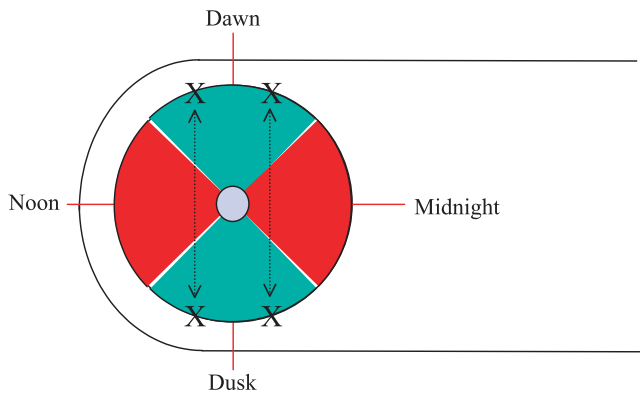

Figure 8. Schematic showing the green region of "allowed" conjunctions. The crosses indicate two possible conjunctions.

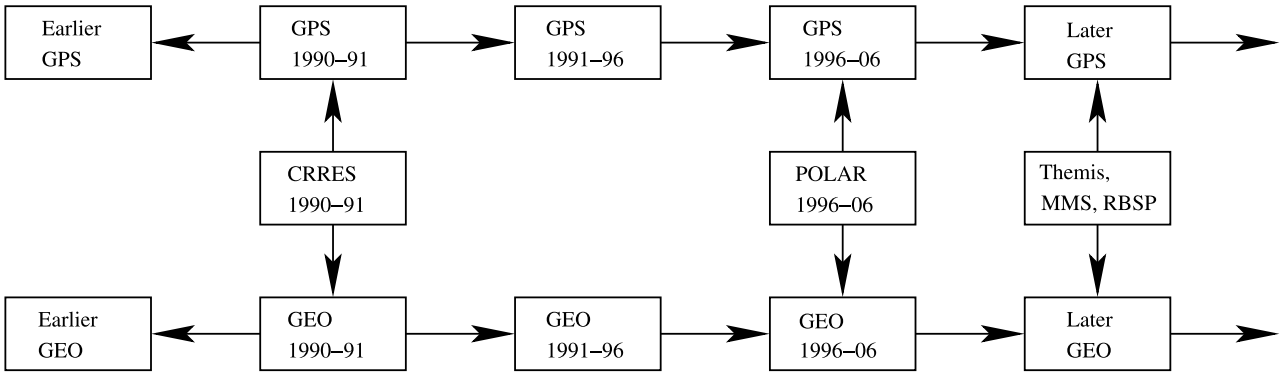

Figure 9. Mission time line for our intercalibration procedure.

could not normally reach provided a good determination of the penetrating background.

[37] Since we cannot obtain any conjunctions between GPS and GEO (they are never at the geomagnetic equator for the same L^*) we independently intercalibrated GEO and GPS with CRRES. Figure 10 shows an example of the matching spectra we obtain between GEO and CRRES, applying the matching factors found. For this pair of satellites the corrections needed were minimal, with correction factors between 0.9 and 1.1, showing that the original calibrations alone were already of good quality.

[38] For the GPS spacecraft, the energy thresholds are gain-dependent, and the gains are known to vary over time, because of both gain drifts and commanding changes in the instruments operation, which changes both the energy assignments of a given channel and the efficiencies for the channel. So here it is not a matter of finding simple adjustment factors for each channel, rather we needed to fit for the correct gain.

[39] Figure 11 shows the result of intercalibrating CRRES with GPS NS18; the red triangles show the raw, uncorrected data and the black crosses the new spectra after adjusting the energy thresholds (gain) to match the CRRES spectra. Added in here is data from the higher-energy HEEF instrument on CRRES, which has been independently intercalibrated to fit with the MEA spectra.

[40] Having established intercalibration factors for GPS and GEO for the CRRES period, the next step was to propagate these calibrations forward and backward in time by defining our GPS/CRRES concurrent mission as the gold standard for GPS, and the GEO/CRRES concurrent mission as the gold standard for LANL GEO.

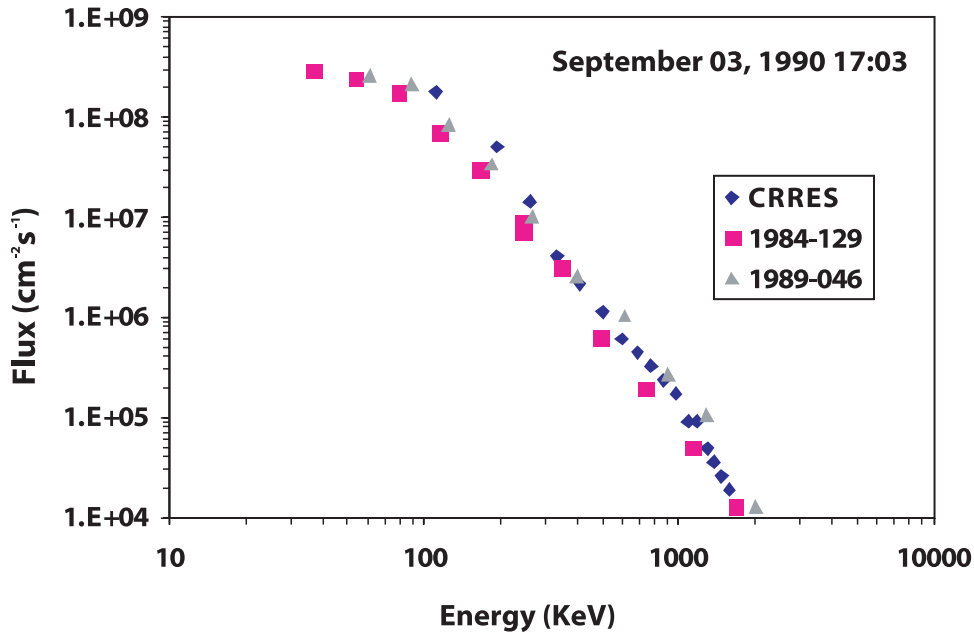

Figure 10. Matching spectra between CRRES and two GEO spacecraft in September 1990. Fluxes are spin averaged and integral above given energy.

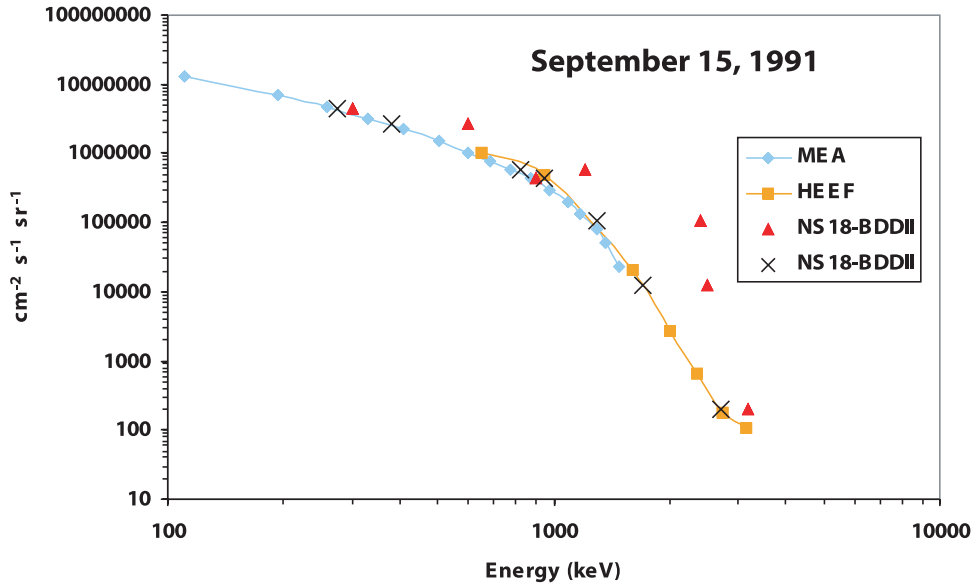

Figure 11. Matching spectra between CRRES and GPS NS18 spacecraft in September 1991. Fluxes are integral above given energy.

[41] Since both GPS and GEO missions always have more than one spacecraft operating at any given time in exactly the same orbits, finding mission overlap and a very large number of conjunctions is no problem. Using this procedure we obtained an intercalibrated set of GPS and GEO data going back to the origin of both of these satellite programs. Propagating the intercalibrations forward in time was also done, but here we now had the opportunity of using another scientific mission with energetic particle instrumentation (Polar CEPPAD) that did have conjunctions with both GPS and GEO to check on how well our original CRRES/LANL/GPS intercalibration stood "the test of time."

[42] Figure 12 shows the intercalibration adjustment required for Polar, for two sample conjunctions. We assumed here that our forward propagated, adjusted GEO data was our gold standard, and found the adjustment factor needed for the Polar spectra to agree.

[43] Shown in blue is the reference spectrum from GEO, comprising the SOPA and higher-energy ESP instrument. The light blue dots are the uncorrected Polar IES spectrum, and the purple squares the uncorrected HISTe spectrum. Overlaid in red is the corrected Polar IES spectrum, and the yellow triangles show the corrected HISTe spectrum, both of which agree well with the GEO reference in both cases, using the same adjustment factors. The adjustment factors used are shown in Table 1.

[44] Now assuming our procedure for intercalibrating the data has been correct up until now, then we would expect that exactly the same adjustment factors as shown in Table 1 should yield a good fit in the spectra when compared to GPS. Figure 13 shows the comparisons of the

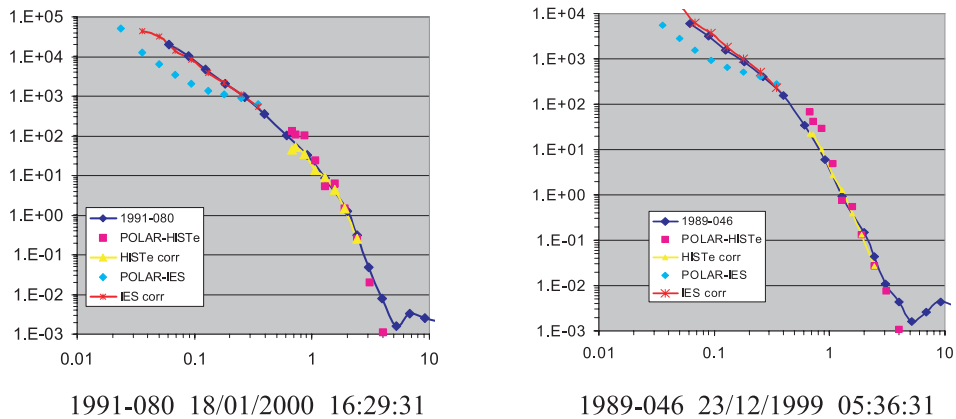

Figure 12. Two examples of matching spectra between GEO and Polar. See text for details.

Table 1. Adjustment Factors for LANL GEO-Polar Intercalibration

Channel	Polar IES	Polar HISTe
1	0.3	
2	0.2	3.0
3	0.25	2.0
4	0.25	2.9
5	0.35	1.8
6	0.5	0.6
7	0.8	1.4
8	1.2	2.0
9		2.0
10		2.0
11		2.0
12		2.0
13		2.0
14		2.0

corrected and uncorrected Polar spectra to two separate GPS satellites when they and Polar are in conjunction, using the factors of Table 1.

[45] GPS ns24 and ns33 during the Polar period have only a few functioning energy channels, as these satellites have been operating for some time and have almost run out of gain adjustment. However, even over the limited overlap in energy we can see a remarkable agreement of the adjusted spectra. Given the long procedure that has lead to this comparison this result is most gratifying indeed, and lends confidence to our intercalibration procedure.

[46] If one takes the view that "scientific" missions such as CRRES and Polar have been in general well characterized and calibrated, then one should be able to take Polar as a "gold standard" in the same way CRRES was used at the beginning of our work. From this point of view the "adjustment" factors of Table 1 could be interpreted as a lower bound of the overall uncertainty in our intercalibration method.

4. Error Sources and Caveats

[47] The success of the full-loop intercalibration from CRRES to Polar via GPS and GEO data is somewhat surprising, as our method makes a range of assumptions and simplifications which should lead to an ever larger propagating error throughout the procedure. Some of these assumptions and error sources are discussed here in turn.

4.1. GEO Calibrations

[48] A more detailed simulation of the LANL geosynchronous SOPA instrument has been performed [*Cayton and Tuszewski*, 2005]. The simulations performed clearly show the effect of Bremsstrahlung on the response of the SOPA energy channels, leading to an overestimation of the counts especially at the lower energy channels. This indicates that our assumption of an energy spectrum independent calibration does not hold, and that the response does to some extend depend on the hardness of the real spectrum. The harder the spectrum, the larger the contribution of Bremsstrahlung to the electron count rate, becoming increasingly more significant even for the higher energy channels. This effect becomes negligible only for soft spectra, which are generally observed during quiet time, so our restriction to periods of $Kp < 2$ for two days before conjunction helps. Requiring this "quiet condition" to have persisted for the previous 2 days is in response to the observed energetic electron dynamics, which often show a peak within two days of an active period [*Reeves et al.*, 2003].

[49] Thus our intercalibration is strictly valid for quiet conditions only, and larger errors are expected during disturbed times. Incorporating the results of [*Cayton and Tuszewski*, 2005] will lead to updated calibrations for the LANL SOPA instruments, which is an ongoing and time consuming task. Once this has been done, the process described here will have to be repeated.

4.2. Spin-Averaged Versus Pitch Angle Resolved Data

[50] All the data used here is in the form of spin-averaged flux data. This is partly by necessity, as instruments on GPS have no directional capability and both GPS and GEO satellites do not carry a magnetometer.

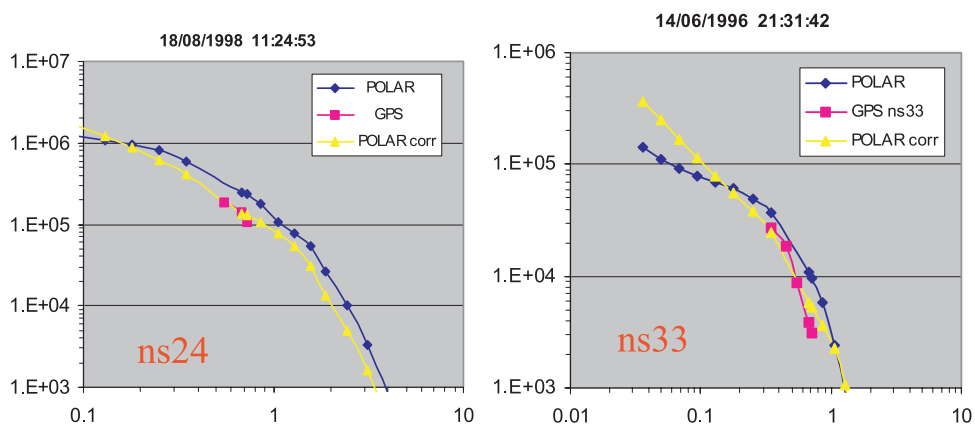

Figure 13. Two examples of matching spectra between GPS and Polar. See text for details.

[51] Our basic assumption in section 2.2 was that particles measured at the same L^* are expected to have the same flux. That is a simplified way of stating Liouville's theorem, which states that along drift trajectories the phase space density (PSD) at constant adiabatic invariants is preserved. Adiabatic invariants correspond to a particle's gyro motion around a field line (first), its bounce along a field line (second) and its drift along its drift shell around the Earth, characterized by L^* (third adiabatic invariant).

[52] However, in real, nondipole magnetic fields L^* is different for different values of the second adiabatic invariants, that is its pitch angle. This phenomenon is called "drift shell splitting" [*Roederer*, 1974] and leads to the fact that not all the same particles observed in one satellite's spin average follow the same drift trajectory [*Reeves et al.*, 1991], and that consequently the spin-averaged sample at another satellites consists of slightly different particles. The L^* used here is for 90° pitch angle particles, generally corresponding to the peak of the particle distribution.

[53] The effects of drift shell splitting and the errors it causes are generally larger for more active periods, for larger L^* values and for large satellite separations, and since we do not know what the real pitch angle distributions are at these satellites, these errors are in principle not quantifiable. Further, the effects of drift shell splitting will be most noticeable when comparing day and night-side pitch angle distributions. At dawn and dusk the effects are much less important [*Selesnick and Blake*, 2002]. Limiting our analysis here to the dawn and dusk quadrants (see Figure 8) already minimizes this effect.

[54] However, the results presented in section 5 show that at least during quiet periods, these errors can be quite small in the geosynchronous region.

4.3. GEO Propagation of Intercalibrations

[55] The GEO spacecraft are more or less uniformly distributed in local time abound the Earth. Because of the dipole tilt and the fact that the satellites corotate with the Earth, this leads to each satellite being consistently at a different average magnetic latitude or B/B_{EQ}, thus sampling a consistently different fraction of the true equatorial particle distribution. Especially for peaked pitch angle distributions this would lead to systematic offsets between satellite's spin-averaged measurements which have nothing to do with any intercalibration issues.

[56] Again, since the differences in magnetic latitude are small this is not a major effect on average, large errors are again only expected during disturbed condition which lead to radically nonisotropic pitch angle distributions.

4.4. Use of Static Magnetic Field Model for L^*

[57] At this point the use of the static Olson Pfitzer 1977 model was motivated by computational speed in calculating L^* for a large numbers of spacecraft positions. The Olson Pfitzer 1977 model is a good average model for the inner magnetosphere, but as the work by *Chen et al.* [2005] has shown even for the most quiet conditions there are consistent deviations between model and data at geosynchronous orbit which are on the order of 10%, with short-duration fluctuation not being reproduced at all.

[58] As our conjunction used include a condition for low activity $Kp < 2$) the use of a static model is somewhat justified. This does however remain a known error source, but one which can only be dressed once high-fidelity, global and dynamic magnetic field models for the inner magnetosphere become available.

5. Testing the Intercalibration at Geosynchronous Orbit

[59] Part of the work of *Chen et al.* [2005] enables us to perform a more rigorous intercalibration between geosynchronous measurements that avoids some of the problems discussed in section 4. *Chen et al.* [2005] make use of a limited, recent set of GEO data that have been sorted into pitch angles using the magnetic field direction derived from the symmetries of the plasma distribution of the MPA plasma instrument on the same satellites [*Thomsen et al.*, 1996]. Using these data it is possible, together with a global magnetic field model, to evaluate the PSD at constant values of all three adiabatic invariants, and to then match data between satellites that are at the same set of adiabatic invariants, thus rigorously fulfilling the conditions of Liouville's theorem. *Chen et al.* [2005] also use the Olson Pfitzer 1977 model and a period where it is shown to fit the existing magnetic field data the best.

[60] Figure 14 shows the resulting intercomparison between two GEO satellites for one quiet day, for a range of energies (μ), for all PSDs observed at both satellites for the same second and third adiabatic invariants for each μ. These PSDs were all calculated on the basis of the intercalibration procedure described in this paper. "Perfect" intercalibration would require all points to lie along a straight line of slope = 1. The fitting curve shown a slope of 1.038, indicating that our intercalibration procedure used does a very decent job indeed.

[61] It must be remembered that our procedure yields an average intercalibration, whereas the procedure developed by *Chen et al.* [2005] does a far more detailed ad hoc intercalibration for a given quiet period. Our statistical method does however provide a starting point for more detailed methods which is already "very close."

6. Other Applications

[62] There have been two further applications to date that have made use of the intercalibrated set of data

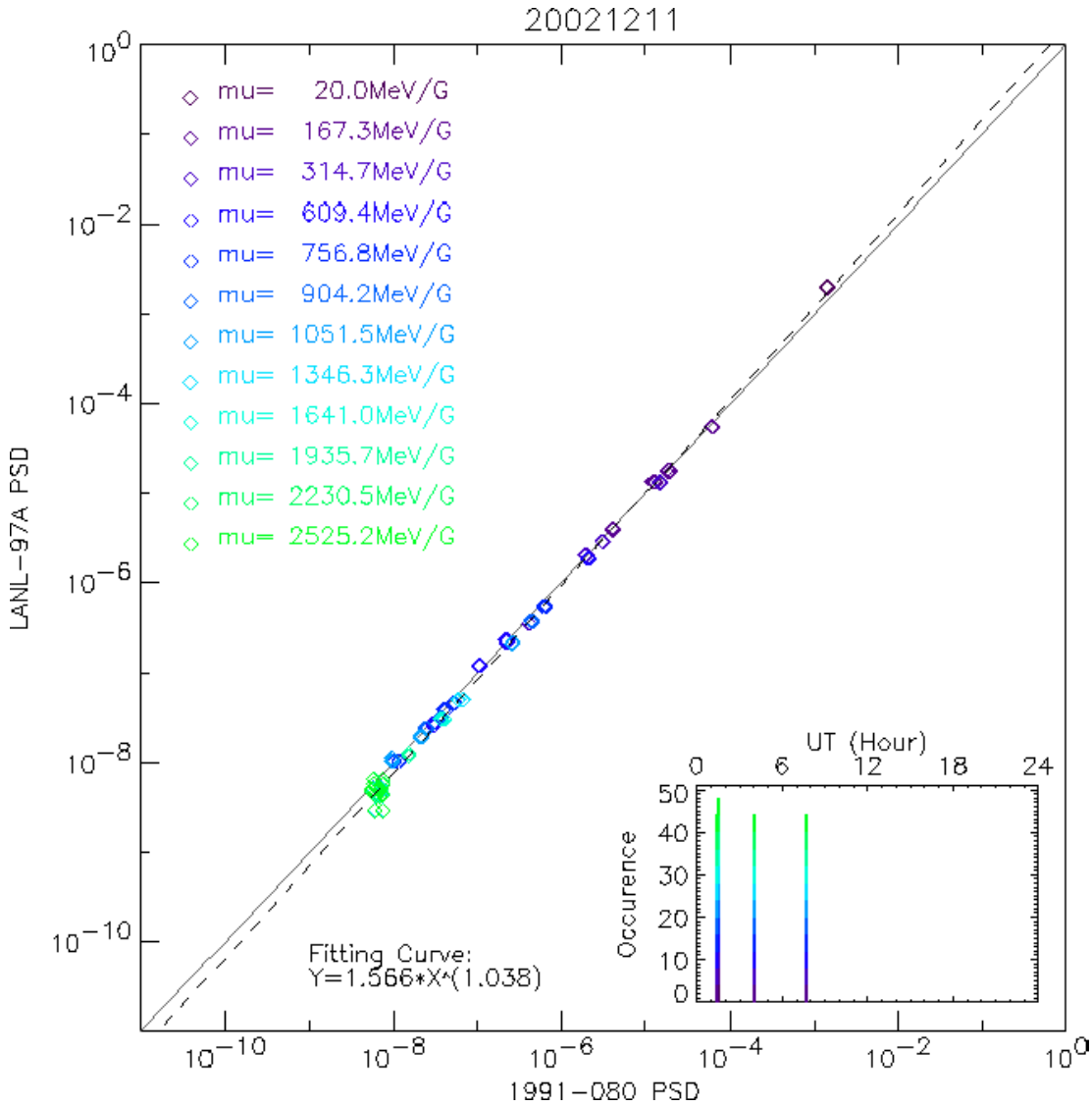

Figure 14. Comparison of phase space densities between two GEO spacecraft for a range of μ at constant second and third adiabatic invariants. The inset shows the number of PSD matching occurrences and the local times at which they occur during the quiet day of 11 December 2002.

produced here. *Boscher et al.* [2003] have used the 30-year span of the intercalibrated GEO data set to construct a solar cycle–dependent model (POLE) of the geosynchronous energetic electron environment. They show that the use of the POLE model versus the industry standard AE-8 in predicting on-orbit solar panel power degradation is much closer to the actually measured power curves. Since AE-8-based models overestimate the actual power loss, use of POLE can lead to substantial savings in solar panel specifications.

[63] *Bourdarie et al.* [2005] have used the intercalibrated GPS and GEO data and a simple data assimilation technique to improve the performance of an existing diffusive radiation belt model (Salammbô [*Bourdarie et al.*, 1996]). They use a nudging technique to update the models simulation cells with data and data-derived information whenever available. Having intercalibrated data for this process is crucial for the model to operate realistically, and not to simply attempt to match ''nonmatching''data through its physical processes.

[64] Using an independent test spacecraft [*Bourdarie et al.*, 2005] could show that the inclusion of data improved model performance significantly, even in the absence of some physical processes in the model that are known to exist but have not yet been incorporated. In this way the Salammbô model can be used to ''extrapolate'' in a phys-

ical way the limited input data to achieve a globally valid representation of the energetic electron environment.

7. Summary

[65] We heave presented here a general method for the intercalibration of energetic electron data in the inner magnetosphere. The method is applied here to CRRES, GPS, GEO and Polar data, but is equally applicable to data from other mission such as HEO and CLUSTER, and future missions such as Themis and MMS (Figure 9). The method developed here has one limitation: it does require equatorial conjunctions between spacecraft, which currently excludes LEO missions such as SAMPEX and NOAA TIROS (intercalibration method for these spacecraft are under development).

[66] By ''closing the loop'' of our intercalibration path from CRRES to Polar with self-consistent intercalibration factors we have demonstrated the validity of our approach for on-orbit intercalibrations. A detailed testing of our intercalibration at geosynchronous orbit showed remarkable fidelity of the intercalibration in spite of the numerous possible error sources discussed in section 4.

[67] Applications of our intercalibrated data set have already yielded a useful new geosynchronous solar cycle–dependent energetic electron environment model, and have been used to improve the performance of a physical radiation belt model through a data assimilation process.

[68] The work described here is very much a ''work in progress.'' As improved instrument response calibrations and improved magnetic field models become available, a lot of the work performed already will have to be revisited. While far from perfect this work has been motivated by a desire to be able to produce the best set of intercalibrated data possible now.

[69] We believe this data set will play an integral role in the production of future statistical radiation belt models, for space weather now casting uses and for scientific understanding of energetic electron processes leading to the development of accurate physical models.

[70] **Acknowledgments.** We thank R. D. Belian, R. A. Christensen, and M. M. Meier for providing assistance with the LANL satellite data and W. Feldman and C. Ingraham for the GPS data. This work was supported by grant W-19,957 from NASA's LWS (Living with a Star) Research and Technology Program and by the U.S. Department of Energy Office of Basic Energy Science (OBES) and ONERA internal funding.

References

Blake, J. B., et al. (1995), CEPPAD: Comprehensive energetic particle and pitch angle distribution experiment on Polar, *Space Sci. Rev.*, *71*, 531–562.

Boscher, D. M., S. A. Bourdarie, R. H. W. Friedel, and R. D. Belian (2003), Model for the geostationary electron environment: POLE, *IEEE Trans. Nucl. Sci.*, *50*, 2278–2283.

Bourdarie, S., D. Boscher, T. Beutier, J. A. Sauvaud, and M. Blanc (1996), Magnetic storm modeling in the Earth's electron belt by the Salammbô code, *J. Geophys. Res.*, *101*, 27,171–27,176.

Bourdarie, S., R. H. W. Friedel, J. Fennell, S. Kanekal, and T. E. Cayton (2005), Radiation belt representation of the energetic electron environment: Model and data synthesis using the Salammbô radiation belt transport code and Los Alamos geosynchronous and GPS energetic particle data, *Space Weather*, *3*, S04S01, doi:10.1029/2004SW000065.

Cayton, T. E., and M. Tuszewski (2005), Revised electron fluxes from the synchronous orbit particle analyzer, *Space Weather*, doi:10.1029/2005SW000150, in press.

Chen, Y., R. H. W. Friedel, G. D. Reeves, T. G. Onsager, and M. F. Thomsen (2005), Multisatellite determination of the relativistic electron phase space density at geosynchronous orbit: 1. Methodology and results during geomagnetically quite times, *J. Geophys. Res.*, doi:10.1029/2004JA010895, in press.

Feldman, W., W. Aiello, D. Drake, and M. Herrin (1985), The BDD II: An improved electron dosimeter for the global positioning system, *Tech. Rep. LA-10453-MS*, Los Alamos Natl. Lab., Los Alamos, N. M.

Friedel, R. H. W., G. D. Reeves, and T. Obara (2002), Relativistic electron dynamics in the inner magnetosphere–A review, *J. Atmos. Terr. Phys.*, *64*, 265–282.

Jordan, C. E. (1994), Empirical models of the magnetospheric magnetic field, *Rev. Geophys.*, *32*, 139–157.

Olson, W. P., and K. A. Pfitzer (1977), Magnetospheric magnetic field modeling, technical report, McDonnell Douglas Astronaut. Co., Huntington Beach, Calif.

Reeves, G. D., R. D. Belian, and T. A. Fritz (1991), Numerical tracing of energetic particle drifts in a model magnetosphere, *J. Geophys. Res.*, *96*, 13,997–14,008.

Reeves, G. D., R. D. Belian, T. C. Cayton, M. G. Henderson, R. A. Christensen, P. S. McLachlan, and J. C. Ingraham (1997), Using Los Alamos geosynchronous energetic particle data in support of other missions, in *Satellite-Ground Based Coordination Source Book*, edited by M. M. Lockwood, M. N. Wild, and H. J. Opgenoorth, *Eur. Space Agency Spec. Publ.*, *ESA-SP 1198*, 263–272.

Reeves, G. D., K. L. McAdams, R. H. W. Friedel, and T. P. O'Brien (2003), Acceleration and loss of relativistic electrons during geomagnetic storms, *Geophys. Res. Lett.*, *30*(10), 1529, doi:10.1029/2002GL016513.

Roederer, J. G. (1974), The Earth's magnetosphere, *Science*, *183*, 37–46.

Selesnick, R. S., and J. B. Blake (2002), Relativistic electron drift shell splitting, *J. Geophys. Res.*, *107*(A9), 1265, doi:10.1029/2001JA009179.

Thomsen, M. F., D. McComas, G. Reeves, and L. Weiss (1996), An observational test of the Tsyganenko (T89a) model of the magnetospheric field, *J. Geophys. Res.*, *101*, 24,827–24,836.

Vampola, A. L., J. V. Osborne, and B. M. Johnson (1992), CRRES magnetic electron spectrometer AFGL-701-5A (MEA), *J. Spacecr. Rockets*, *29*, 592–594.

S. Bourdarie, Centre d'Etudes et de Recherches de Toulouse, Département Environnement Spatial, Office National d'Etudes et de Recherche Aérospatiales, BP 4025, 2, Avenue Edouard Belin, F-31055 Toulouse Cedex 4, France. (sebastien.bourdarie@onecert.fr)

T. E. Cayton and R. H. W. Friedel, Los Alamos National Laboratory, P.O. Box 1663, Los Alamos, NM 87545, USA. (tcayton@lanl.gov; friedel@lanl.gov)